4.6

Reprinted from Preprint Volume: Nineteenth Conference on Radar Meteorology, April 15-18 1980, Miami, Fla.
Published by the American Meteorological Society, Boston, Mass.

COMPARISON OF AIRBORNE AND LAND-BASED RADAR MEASUREMENTS OF PRECIPITATION DURING THE WINTER MONSOON EXPERIMENT

by

R.A. Houze, Jr.[1], S.G. Geotis[2], F.D. Marks, Jr.[2], and D.D. Churchill[1]

[1]Department of Atmospheric Sciences
University of Washington
Seattle 98195

[2]Department of Meteorology
Massachusetts Institute of Technology
Cambridge 02139

1. INTRODUCTION

During the International Winter Monsoon Experiment (Winter MONEX), conducted in Malaysia during December 1978 - January 1979 (Greenfield and Krishnamurti, 1979), the WP3D instrumented aircraft of the NOAA Research Facilities Center was based at Kuala Lumpur, on the Malay Peninsula (West Malaysia), and the WR73 weather radar system of the Massachusetts Institute of Technology (MIT) was located at Bintulu, Sarawak, on the northern coast of Borneo (East Malaysia). The WP3D aircraft is equipped with weather radars in its nose, tail and lower fuselage. On one of its research missions over the South China Sea, the WP3D aircraft flew within range of the MIT radar, allowing a comparison to be made between the echo patterns shown by the airborne and land-based radar systems. In a previous comparison, Jorgensen and Lewis (1978) showed that the echo pattern obtained with the WP3D lower fuselage radar in a hurricane was qualitatively consistent with an echo pattern shown by the WSR-57 radar of the National Weather Service in Brownsville, Texas. In this paper, we compare the quantitative reflectivity patterns obtained with the WP3D lower fuselage radar and the MIT radar during the Winter MONEX comparison flight.

2. CHARACTERISTICS OF THE RADAR SYSTEMS

Both the WP3D lower fuselage radar and the MIT radar operate at C-band, and the signals of both radars are digitally processed. Characteristics of both systems are listed in Table 1. The digital processing on the WP3D is accomplished with a Digital Video Integrator Processor (DVIP), which averages signals according to the method of Sirmans and Doviak (1973). The MIT radar system uses an on-line minicomputer to control the direction of the antenna and to carry out all signal processing, averaging and recording functions.

In addition to the characteristics listed in Table 1., the WP3D lower fuselage radar antenna is stabilized with respect to the pitch and roll of the aircraft. Further details of the WP3D weather radar systems can be found in Jorgensen and Lewis (1978).

Table 1. Radar System Characteristics

	MIT WR73 Radar	WP3D Aircraft Lower Fuselage Radar
Wavelength	5.30 cm	5.59 cm
Pulse length	300 m	900 m
PRF	250 s^{-1}	200 s^{-1}
Peak Power	250 kW	70 kW
Horizontal beam width	1.45°	1.1°
Vertical beam width	1.45°	4.1°
Azimuth averaging interval	1.0°	1.8°
Azimuth recording interval	1.0°	0.5°
Range bin size	0.25-1.0 km	1.45 km
Maximum range recorded	256 km	379 km

The MIT radar was used to obtain three-dimensional reflectivity patterns throughout the field phase of Winter MONEX. The three-dimensional patterns were obtained by running the antenna through a sequence of conical scans every 10 min, each sequence taking about 8 min to complete. This procedure was carried out from 8 December 1978 to 1 January 1979, providing a continuous record of the three-dimensional echo structure over the North Borneo coast and adjacent South China Sea region for almost a month. There were no significant interruptions in the data collection during this time.

3. LOCATION AND METEOROLOGICAL SETTING FOR THE INTERCOMPARISON

The path of the WP3D aircraft through the region of coverage of the MIT radar during the intercomparison flight on 16 December 1978 is indicated in Fig. 1. We will concentrate on the portion of the flight between points A and B.

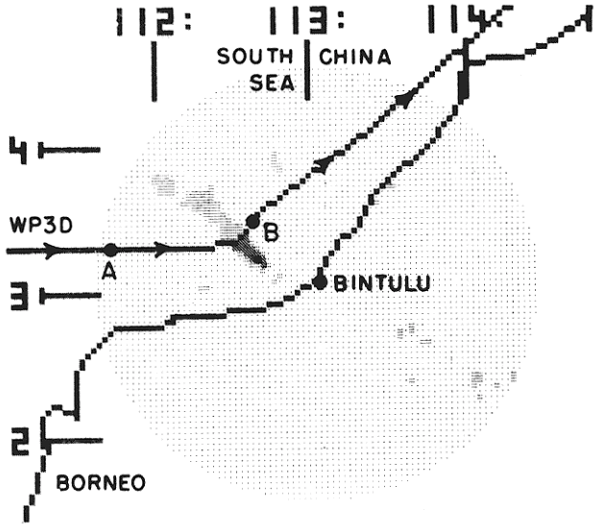

Figure 1. Region of the intercomparison. Shaded circle is the area covered by the MIT radar located at Bintulu on the north coast of Borneo. Line with arrow shows the path of the NOAA WP3D aircraft over the South China Sea. Intercomparison is made for the portion of the flight between A and B. The low-level radar echo pattern (CAPPI for 2 km altitude inside 170 km range) from the MIT radar is shown. Thresholds for the echo shadings are 15, 30 and 40 dBZ.

During this time, the aircraft approached and penetrated the line of echo extending northwestward from the MIT radar site at Bintulu.

The aircraft was flying at an altitude of 6.8 km, below an extensive layer of stratiform cloud. In satellite imagery, this cloud layer had the appearance of a large cirriform anvil, typical of equatorial latitudes. It was associated with convection which regularly forms along the Borneo coast at night during the winter monsoon. As this convection matures during the night a widespread anvil develops. As the anvil widens, the precipitation from it becomes primarily stratiform. The anvil and its stratiform precipitation are usually located northwest of Bintulu and are best defined at about 0800 LST. After that time the anvil and the stratiform precipitation slowly dissipate during the remainder of the day. This nocturnally generated precipitation system will be described in detail in a forthcoming paper. By the time the aircraft was located at point A in Fig. 1, the upper-level stratiform cloud layer with some virga falling from it was all that remained of this cloud system. The line of convection seen in Fig. 1 was a new development, which appeared in the morning, while the nocturnal feature was dissipating. The virga from the upper-level anvil cloud does not appear in the low-level echo pattern in Fig. 1 since it was evaporating before reaching the surface. The virga appears in the echo patterns at higher levels on both the MIT and WP3D radars, as will be seen in subsequent figures.

4. ECHO PATTERNS DETECTED WITH THE AIRBORNE RADAR

A sequence of the echo patterns from the aircraft's lower fuselage radar are shown in Fig. 2. The virga from the dissipating anvil is the region of uniform echo, some 25 km x 60 km in

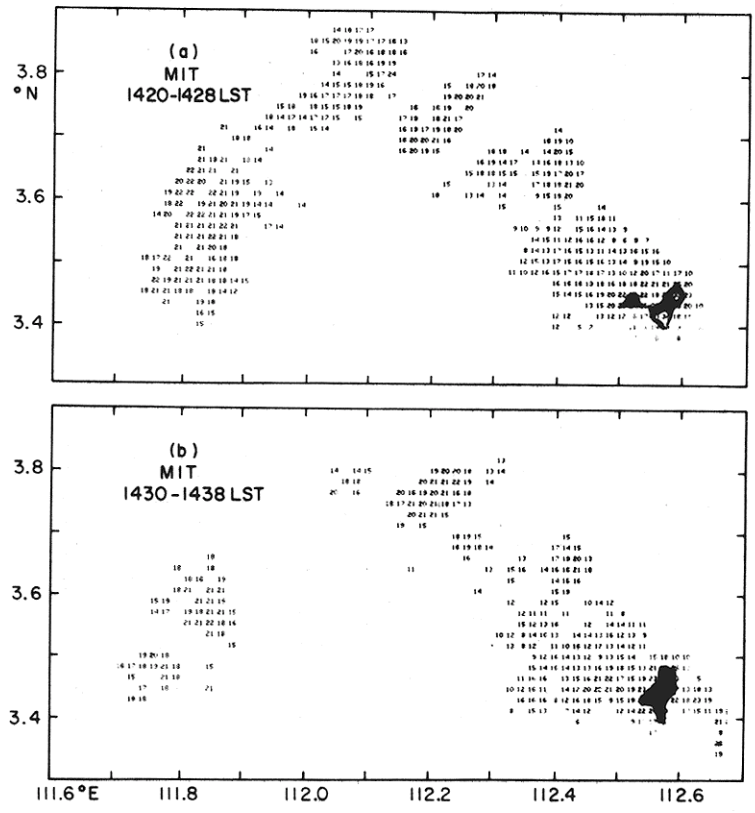

Figure 3. Echo patterns for the 6.8 km level shown by the MIT land-based radar. Echo contours are drawn from 2 km x 2 km x 2 km resolution data for 25 and 30 dBZ. In (a) and (b) the patterns are constructed from the three-dimensional scans for 1420-28 LST and 1430-38 LST, respectively.

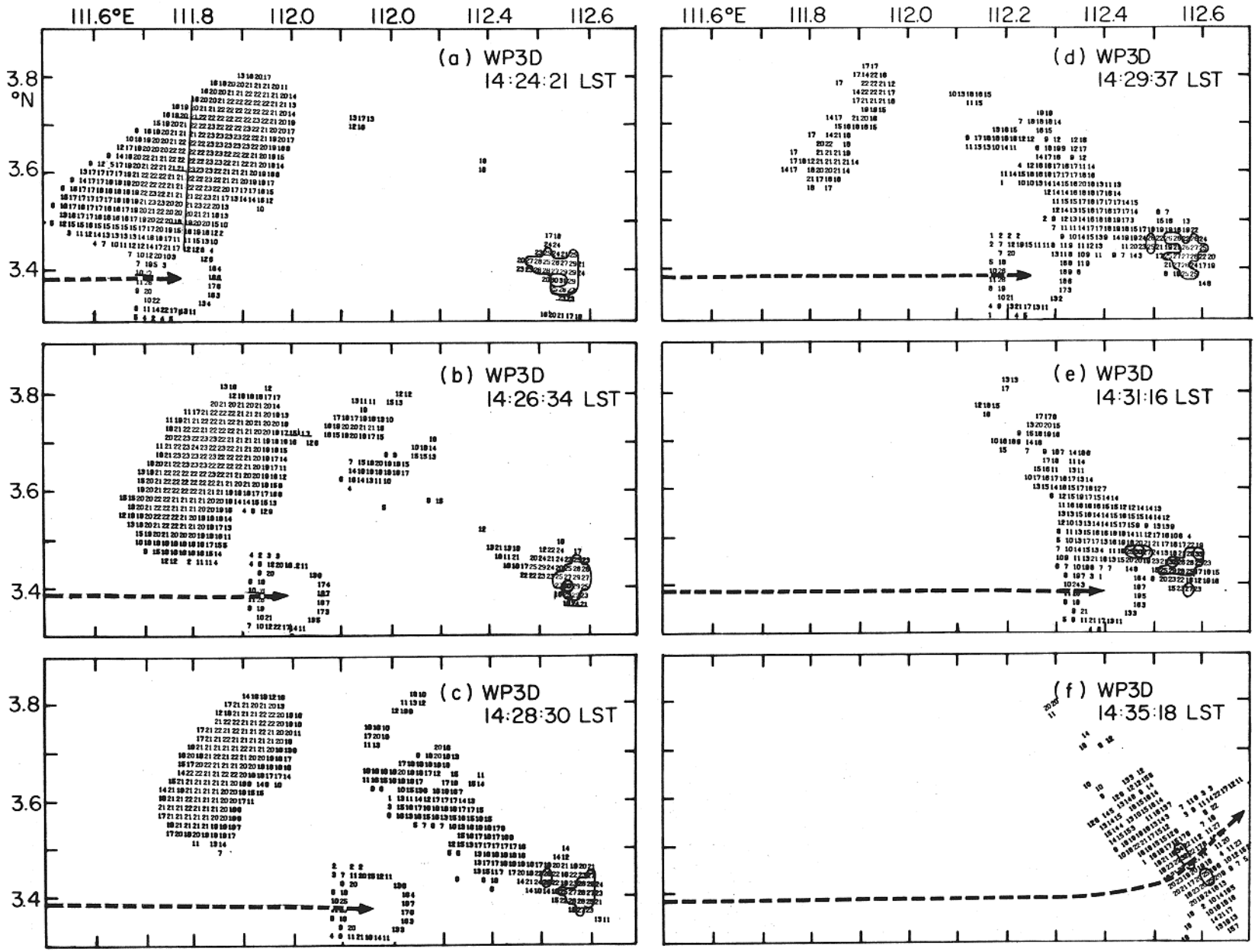

Fig. 2 Sequence of echo patterns shown by the lower fuselage radar of the WP3D aircraft. Path of aircraft up to the time of the map is indicated by the dashed arrow. Contours are for 25 and 30 dBZ. Circle of echo around aircraft is from sea surface.

dimension, seen just north of the aircraft in Fig. 2a. The horizontally uniform appearance of the virga is characteristic of the stratiform anvil precipitation associated with the nocturnal cloud system.

At this time, the line of convection to the east of the aircraft was just becoming evident. The strong cellular echo at the southeastern end of the line, composed mostly of echo of 25-30 dBZ, was clearly seen, with two smaller weaker echoes evident to its northwest, between the cellular echo and the region of virga. As the aircraft approached the line, its full extent became apparent (Figs. 2b-e). Except for the cells at its southeast end, the echo line was composed of fairly weak echo, generally < 20 dBZ. At the time of Fig. 2a, most of this weaker echo was below minimum detectable intensity. As the distance between the aircraft and the band decreased, the portion of the line with echo exceeding the minimum detectable signal quickly increased. The substantial change in appearance of the convective echo line between Figs. 2a and 2c occurred over a time interval of only 4 min. This change illustrates how rapidly the appearance of a portion of the airborne radar echo pattern can change from one of isolated cells to one of an organized mesoscale line.

As the aircraft moved toward the convective line, the echo from the virga falling from the anvil decreased quickly in size (Figs. 2a-2d). By the time of Fig. 2e, the region of virga had disappeared. This change may have been partly an effect of the aircraft moving away from the echo. Since the virga did not extend very far below the aircraft's flight level, it probably filled a rapidly decreasing fraction of the 4.1° vertical beamwidth as the aircraft moved away from the region of virga. The change in the appearance of the virga, however, was at least partly meteorological. The MIT radar data confirm that the region of virga was diminishing in size and actually disappeared between 1420 and 1440 LST.

The convective echo line was penetrated by the aircraft between 1433 and 1435 LST in the region of the strong cellular echo in the southeastern end of the line. The peak updraft speed encountered by the aircraft was 5 m s^{-1}. The cloud liquid water content (measured by a Johnson-Williams meter) reached 0.11 g m^{-3}. The flight level temperature was -9°C and the precipitation particles (sensed by a Particle Measuring System 2-D probe) in the 0.2 mm-6.4 mm size range were predominantly lumps of graupel. The echo pattern after the penetration is shown in Fig. 2f.

5. ECHO PATTERNS DETECTED WITH THE LAND-BASED RADAR

The echo pattern from the MIT radar at Bintulu (Fig. 3) contained the same features as were seen in the radar echo pattern of the WP3D aircraft. The virga from the anvil cloud is seen near 3.6 °N, 111.8 °E, and the convective line extends from 3.4 °N, 112.6 °E to 3.9 °N, 112.0 °E. Comparison of Figs. 3a and b shows the weakening of the virga which was taking place during that time.

6. COMPARISON OF THE AIRBORNE AND LAND-BASED REFLECTIVITY PATTERNS

a. Anvil Precipitation

A detailed representation of the echo from the virga falling from the anvil is shown in Fig. 4a, which contains a Constant Altitude PPI (CAPPI) map constructed from the three-dimensional scan obtained with the MIT land-based radar between 1420 and 1428 LST (same time as Fig. 3a). This map shows the virga at a height of 6.8 km, which corresponds to the aircraft's flight level. The horizontal and vertical resolution of the maps is 2 km. The virga, as detected by the airborne radar at 1424 LST (same time as Fig. 2a) is shown in detail in Fig. 4b. The horizontal resolution

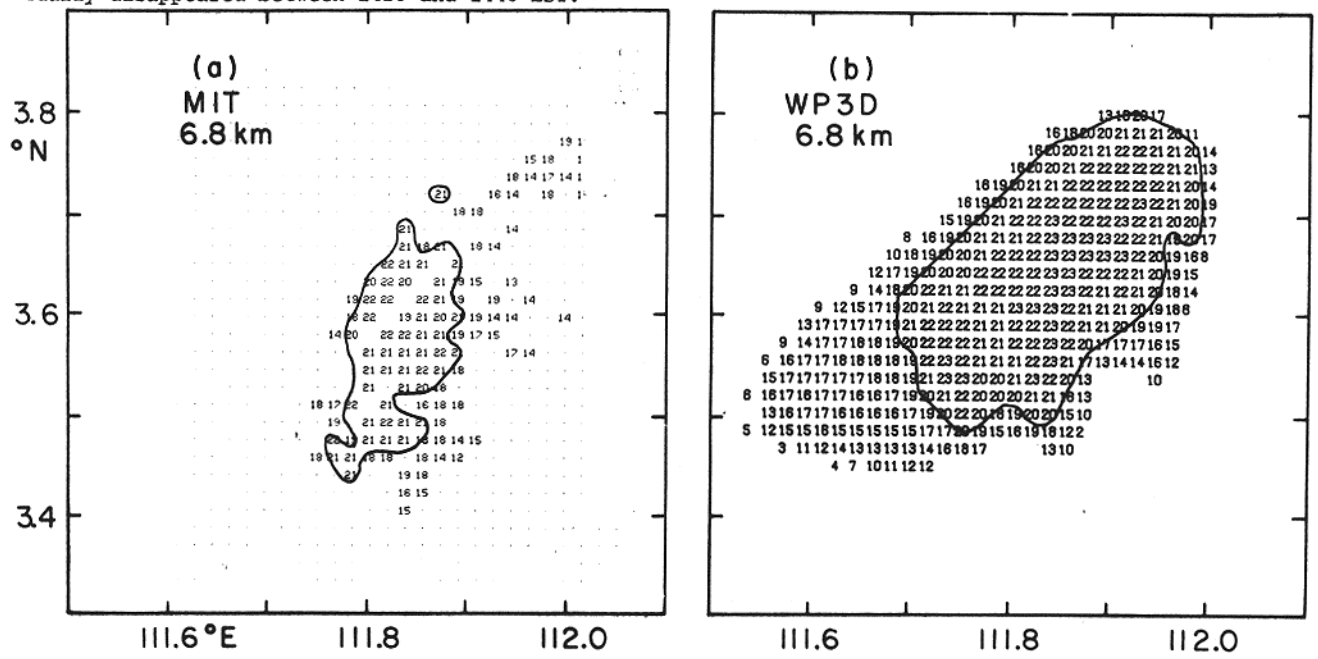

Figure 4. Constant altitude (CAPPI) map from MIT radar for 6.8 km, respectively, is shown in (a). Horizontal and vertical resolution is 2 km. The CAPPI is constructed from 3-D data collected between 1420 and 1428 LST. WP3D lower fuselage radar data obtained at flight level 6.8 km at 14:24:21 LST are shown in 2 km horizontal resolution in (b). Contours are at 20 dBZ.

of the maps is 2 km, but the vertical resolution, determined by the 4.1° vertical beamwidth of the airborne radar, varies within the virga region from 0.5 km in the south corner of the region (closest to the aircraft) to 3.5 km at its northern end (farthest from the aircraft).

The differences in vertical resolution between the two radars, the distance of the MIT radar from the echo (140 km) compared to the close proximity of the aircraft to the echo, and the fact that the MIT patterns are constructed from a lengthy (8 min) conical scan sequence obtained during a time when the echo was changing rapidly in time, all indicate that the horizontal distributions of reflectivity from the two radars cannot be expected to match in detail. However, it is reasonable to seek statistical agreement between the land-based and the airborne radar measurements. Fig. 5 shows that the reflectivity values from the two radars indeed have similar frequency distributions, with the airborne values being most frequent at 22 dBZ while the land-based values were most frequent at 21 dBZ. Thus, we conclude that the two radars agreed to within about 1 dB in the reflectivity of the anvil precipitation. Better agreement could hardly be expected from the two radar systems. The lesser extent of the anvil echo, as sensed by the MIT radar (Fig. 4), is undoubtedly a result of the fact that much of the precipitation was too weak to be detected. The echo mass in the middle of the MIT pattern in Fig. 4a is centered within the strongest portion of the echo detected by the aircraft (Fig. 4b); however, the weaker fringes of the echo do not appear on the MIT radar pattern.

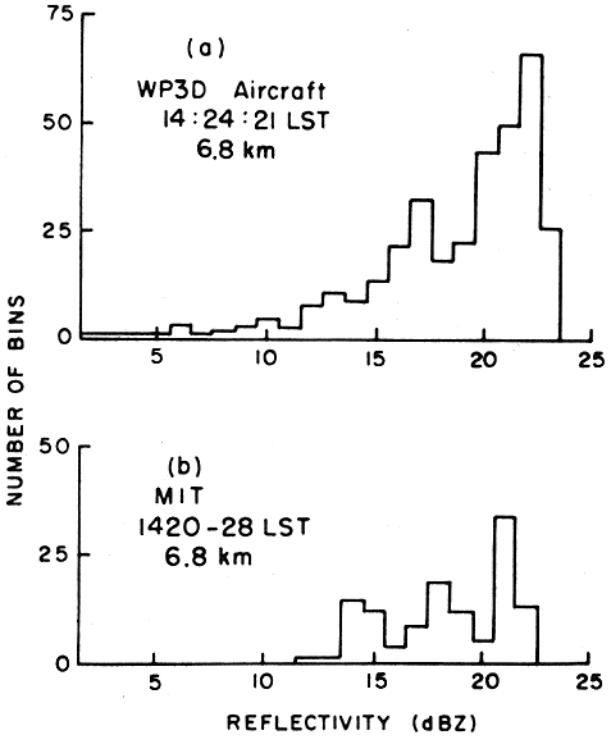

Figure 5. Frequency of occurrence of reflectivities in 2 km x 2 km horizontal data bins in anvil precipitation as detected by WP3D and MIT radars. Data in (a) are from Fig. 4a. Data in (b) are from Fig. 4b.

At the range of this echo from the MIT radar, the minimum detectable signal is about 17 dBZ. From Figs. 4a and 5a it is apparent that a sizable portion of the echo detected by the aircraft flying close to the echo was composed of echo weaker than 17 dBZ.

b. Convective Line

The convective echo line penetrated by the aircraft is shown in CAPPI maps for the MIT radar for the 6, 7 and 8 km levels in Fig. 6a-c and in a detailed map from the airborne radar in Fig. 6d. The horizontal resolution of all of the maps is 2 km. The vertical resolution of the CAPPI maps is also 2 km. The vertical resolution of the aircraft map varies with distance from the aircraft, from about 0.5 km at the echo's closest point to the aircraft to about 3.5 km at its most distant point (northwest of the aircraft).

The convective echo line extended through a deeper layer of the atmosphere, was changing its gross structure less rapidly in time and was located nearer the MIT radar than the virga echo examined in the last section. Consequently, the patterns in the convective line echo detected by both radars, despite their different beam geometries and sampling schemes, were very similar in

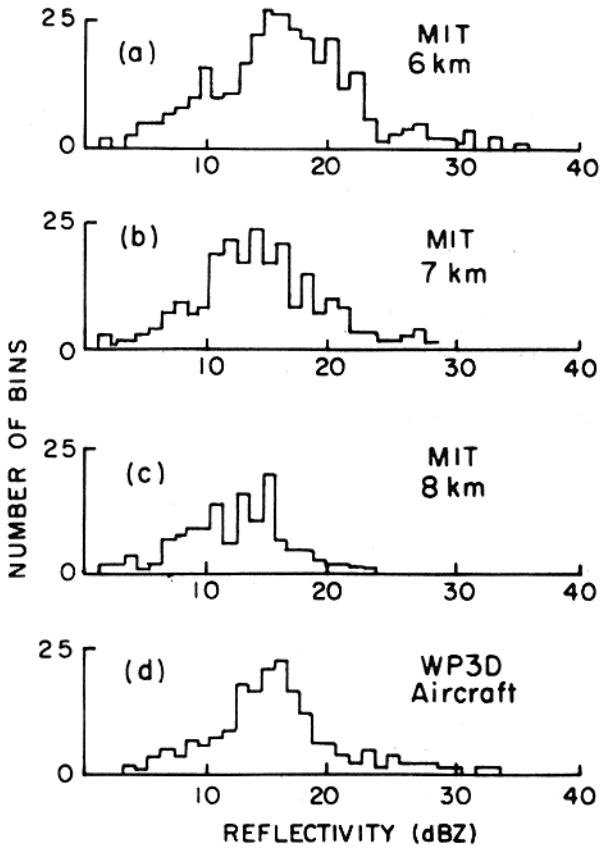

Figure 7. Frequency of occurrence of reflectivities in 2 km x 2 km horizontal data bins in the convective line as detected by WP3D and MIT radars. Data in (a) - (d) are from Figs. 6a - 6d, respectively.

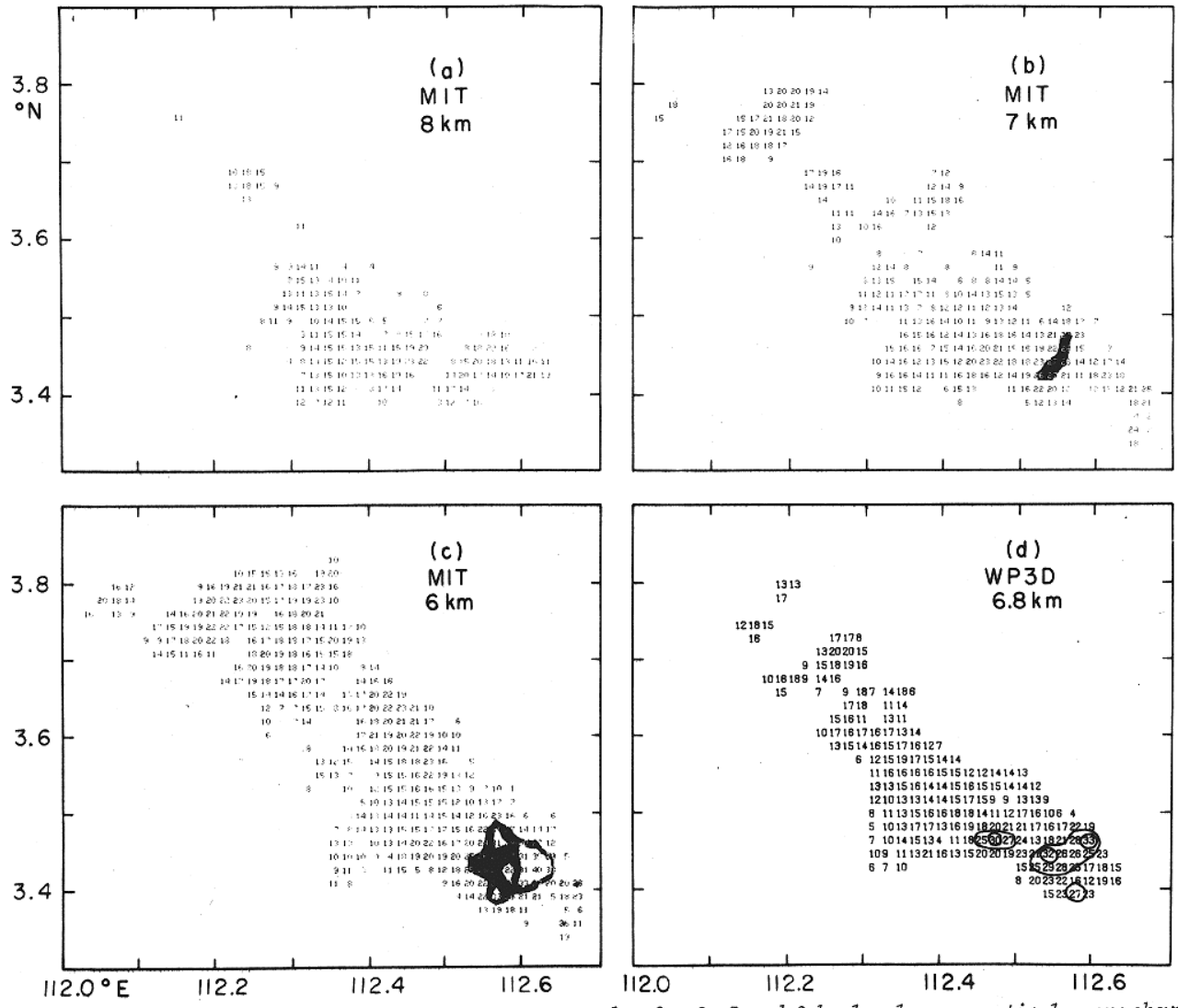

Figure 6. Constant altitude (CAPPI) maps from MIT radar for 6, 7 and 8 km levels, respectively, are shown in (a) - (c). Horizontal and vertical resolution is 2 km. CAPPI's are constructed from 3-D data collected between 1430 and 1438LST. WP3D lower fuselage radar data obtained at flight level 6.8 km at 14:31:16 LST is shown in 2 km horizontal resolution in (d). Contours are at 25 and 30 dBZ

both size and in detail. Comparison of Fig. 6b (the CAPPI corresponding closest in altitude to the flight level) and Fig. 6d shows the good agreement between the airborne and land-based echo patterns in size and shape of the overall echo, the location of intense cellular regions within the general echo, and in the magnitudes of the reflectivities.

Comparison of the reflectivity values is aided by Fig. 7, which shows frequency distributions of reflectivities in the convective line. The more varied texture of the convective line than that of the more stratiform anvil precipitation gives these distributions greater spread and more symmetry than those associated with the virga (Fig. 5). Both the central value and spread of the frequency distribution for the airborne radar (Fig. 7d) lie between those of the 6 km and 8 km CAPPI maps from the land-based radar (Figs. 7a, b) and the distribution for the CAPPI map corresponding most closely to flight level (7 km) (Fig. 7c) is quite similar to the distribution for the airborne map. The mean value of the distribution for the airborne radar is 19.9 dBZ. This value is 2 dB greater than the mean of the 7 km CAPPI curve, which is 17.8 dBZ. The mean values for the 6 km and 8 km CAPPI curves of 22.4 and 15.4 dBZ, respectively, bracket the value for the airborne radar. Again, agreement between the two radar systems is quite satisfactory.

7. CONCLUSIONS

Quantitative comparison of reflectivities measured with the WP3D lower fuselage radar and the MIT WR73 weather radar system in two different types of echo features observed during Winter MONEX shows that the two radar systems agreed to within a decibel or two. We consider this near agreement to be excellent and feel confident in proceeding to use the WP3D radar data quantitatively in other MONEX research.

The result of this first quantitative test of the WP3D radar system should also be encouraging to other investigators, who may wish to use the WP3D measurements quantitatively. The intercomparison described here, however, is the only one so far completed and it would be most helpful to conduct further quantitative comparisons to determine

on a broader statistical basis the accuracy of the measurements. These comparisons can be made with any coastal or shipborne weather radar that is instrumented for digitally processing and recording reflectivity measurements and whose calibration is well-established. It is important though that the surface-based radar scan three-dimensionally in space, as the MIT radar did in the present study. Because of the complex beam geometry associated with the large vertical beamwidth of the airborne radar, its vertical resolution has a large variation in space, and real precipitation systems, such as those in the present study, often have steep vertical gradients of reflectivity, which combine with the varying vertical resolution of the airborne radar to give complicated reflectivity patterns. The effects of the variable vertical resolution of the airborne radar echo patterns is further complicated by the rapid motion of the plane, which on approaching or leaving an echo can make the echo's appearnace undergo large changes in a matter of minutes. From the three-dimensional coverage of a surface-based radar, however, the reflectivity patterns shown by the airborne can be placed into spatial context and their quantitative consistency can be assessed.

Acknowledgements

The cooperation of the Airborne Mission Scientist, Dr. Peter J. Webster, and of the pilots and crew of the WP3D aircraft made this study possible. We would also like to thank Billy Lewis for his help with the WP3D data. The research was supported by the Global Atmospheric Research Program, Division of Atmospheric Sciences, National Science Foundation under grant ATM78-00232.

References

Greenfield, R.S. and T.N. Krishnamurti, 1979: The Winter Monsoon Experiment -- Report of December 1978 field phase. Bull. Amer. Meteor. Soc., 54, 439-444.

Jorgensen, D. and B.M. Lewis, 1978: The precipitation structure of Hurricane Anita (1977) as revealed by quantized airborne radar. Preprint Volume, 18th Conf. on Radar Meteor., Amer. Meteor. Soc., Boston, 34-39.

Sirmans, D. and R.J. Doviak, 1973: Meteorological radar signal intensity estimation. NOAA Tech. Memo., ERL NSSL-64, 80 pp.